

COVER PAGE

Document downloaded by @DAEL

Fri Nov 27 02:38:39 2026
For personal use

When automatic English translation is provided, only the original document is authentic.
The EAA cannot be held responsible of any translation error

Bibliographical reference

Bonding Characterization of a Three-Layer Metal-Adhesive-Metal Using Shear Horizontal Modes of Close Dispersion Curves, Damien Leduc, Mounsif Ech-Cherif El-Kettani, Latifa Attar, Mihai Valentin Predoi and Pascal Pareige, Acta Acustica **vol. 103** (Number 6), 2017, pp. 926-931

DOI
https://doi.org/10.3813/AAA.919121

Acta Acustica united with Acustica
Vol. 103 (2017) 926 – 931

DOI 10.3813/AAA.919121

Bonding Characterization of a Three-Layer Metal-Adhesive-Metal Using Shear Horizontal Modes of Close Dispersion Curves

Damien Leduc[1)], Mounsif Ech-Cherif El-Kettani[1)], Latifa Attar[1)], Mihai Valentin Predoi[2)], Pascal Pareige[1)]

[1)] LOMC UMR CNRS 6294, University of Normandy, 76600 Le Havre, France.
damien.leduc@univ-lehavre.fr

[2)] Department of Mechanics, Polytechnic University of Bucharest, Bucharest, Romania

Summary

This work presents numerical and experimental results on the evaluation of the quality of bonding in a metal-adhesive-metal three-layer structure using shear horizontal (SH) guided waves. The studied samples have different levels of adhesion. A numerical finite element simulation based on the Jones model permits to predict the dispersion curves in the different cases. An experimental study, based on a generation of waves by an EMAT transducer and a reception by a piezocomposite transducer, is performed. Results show that a criterion on the quality of the bonding can be found when the quality of the adhesive is degraded by addition of grease in the adhesive, based on the simultaneous propagation, or not, of two close wavenumber-frequency modes of the three-layer.

PACS no. 43.35.Cg, 43.35.Zc

1. Introduction

Bonding has become a common technology in the last decades, especially to assembly composite made parts [1]. Inspecting the bond quality remains a research topic and ultrasonic guided waves are a recent promising alternative, as a particular case of ultrasonic waves which are widely used in non-destructive testing and evaluation (NDT/NDE) [2, 3, 4]. Bulk longitudinal [5] and shear waves, as well as Lamb [6] and shear horizontal (SH) guided waves [7, 8] have been used to investigate the bonding quality. R. Adams and B. Drinkwater have classified the main bonding defects and their detectabilty [9]. A particular attention has been given to Lamb-type waves by many authors [10, 11, 12, 13, 14], due to their relatively long propagation distance. Detectability of kisssing bonds [15] overlaping plates [16] or defects in bonded mechanical parts [17] were also addressed.

Mathematical models of the bond as a distribution of springs were used first by J.P. Jones [18] for guided modes and other models were used for the adhesive-solid interface [19, 20]. Some of these models were used in Finite Elements Method (FEM) simulations of SH propagation [21], Lamb modes [22, 23, 24]. Coupling numerical models with experiments, the inverse problem of determining the adhesive properties was solved [25, 26]. The adhesives are sensitive to fluids contamination, so that dry contact experimental techniques like the ElectroMagnetic Acoustic Transducers (EMAT) are widely used in this context [27, 28, 29].

The present paper continues and extends recent work [30, 31, 32] on bond quality using SH waves, providing a numerical simulation using FEM and an experimental validation of SH-type guided wave propagation in a three-layer structure (metal-adhesive-metal), for which the bonding strength is degraded by addition of grease in the adhesive. It is shown that a criterion can be defined, which can indicate the coupling quality between the substrates. It is based on the simultaneous propagation of SH guided modes, for which the dispersion curves are very close, but distinct. To the authors knowledge, no previous work has been reported about this method, which allows to check the bonding quality between two layers.

2. Samples description

The studied samples are made of 4 mm thickness plane plates of aluminum, bonded with 0.5 mm thickness adhesive layer. A reference sample with an adhesive film of araldite (called araldite 100% or A100 in the following) is compared to other samples in which the araldite is mixed with grease at different volume percentages: 10% (called A90G10), 30% (A70G30) and 50% (A50G50), degrading progressively the adhesive quality and the coupling between the substrates. The measured parameters of the

Received 19 May 2017,
accepted 28 September 2017.

© S. Hirzel Verlag · EAA

Table I. Shear velocity, density and thickness of the studied materials.

	Shear velocity	Density	Thickness
Grease	506 m/s	1107 kg/m^3	
Aluminum	3100 m/s	2800 kg/m^3	4 mm
A100: araldite	1356 m/s	1160 kg/m^3	0.5 mm
A90G10: mixing of 90% of araldite and 10% of vacuum grease	1055 m/s	1155 kg/m^3	0.5 mm
A70G30: mixing of 70% of araldite and 30% of vacuum grease	793 m/s	1144 kg/m^3	0.5 mm
A50G50: mixing of 50% of araldite and 50% of vacuum grease	664 m/s	1134 kg/m^3	0.5 mm

grease are given in Table I. The density of the mixture araldite/grease is calculated as in the case of a perfect gas by

$$\rho_{eq} = \big(1-p\big)\rho_{\text{glue}} + p\rho_{\text{grease}}, \tag{1}$$

in which p is the grease ratio and ρ the density. The shear velocity in the mixture is calculated by the relation

$$v_T = \sqrt{\frac{\mu_{eq}}{\rho_{eq}}} \tag{2}$$
$$= \sqrt{\frac{\mu_{\text{glue}}\mu_{\text{grease}}}{\big[p\mu_{\text{glue}} + (1-p)\mu_{\text{grease}}\big]\big[(1-p)\rho_{\text{glue}} + p\rho_{\text{grease}}\big]}},$$

using mixture laws as in [29]. μ is the Lamé's second parameter. The obtained values for the different samples are gathered in Table I, and are used to calculate their related dispersion curves for comparison with the experimental results.

3. Dispersion curves

A one-dimensional SAFE (Semi Analytical Finite Element) rheological model (Jones [19]) of the interface substrate/adhesive is solved using Comsol software [33]. The two bonded interfaces are replaced by a distribution of springs, working in shear [20]. A representation of this rheological model is given in Figure 1. The two interfaces are the same so we note $R_T = R_{T1} = R_{T2}$. Depending on the stiffness RT of the springs, one can represent the strength of the adhesion between the substrate and the adhesive. In the case of perfect bonding, the value of the stiffness of the spring RT is considered to be infinite and in the case of total delamination to a zero value. This numerical model allows to provide numerically the eigenvalue problem, associated to the wave equation and the boundary conditions. For each frequency, the eigenvalues, which represent the wavenumbers of the SH modes, are calculated (blue dots on Figure 2). It gives the dispersion curves of the studied three-layer structure (represented by its cross-section), assuming for example $R_T = 10^{16}$ N/m^3 for the two interfaces and structure in vacuum [34]. The structure appears as two aluminum plates (each of thickness $h = 4$ mm) more or less coupled according to the quality of the bonding. We observe a splitting of the modes around the Lamb modes of a plate of thickness h, that is to say that in the same frequency range, the number of modes

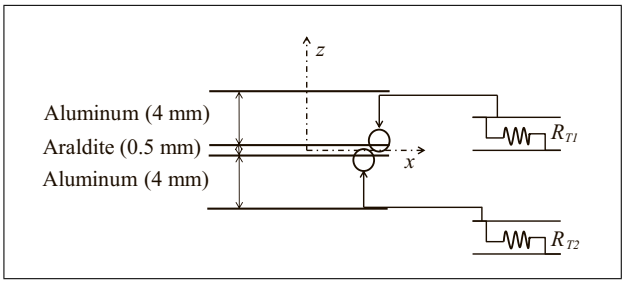


Figure 1. Representation of the Jones model. The sample is a three-layer aluminium-araldite- aluminium.

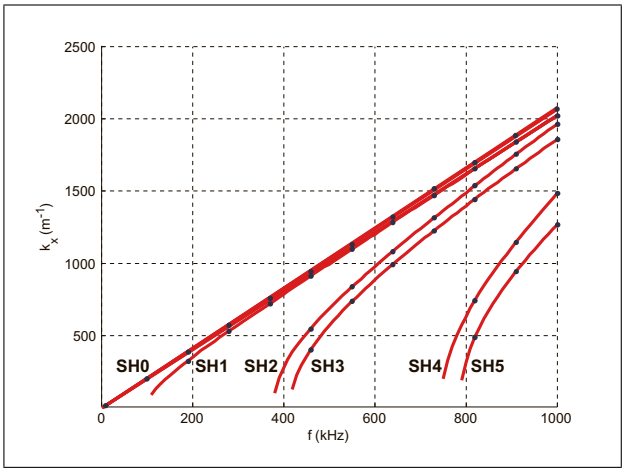


Figure 2. (Colour online) Theoretical dispersion curves in the perfect adhesion hypothesis (red lines). Numerical dispersion curves (Jones model) for $R_T = 10^{16}$ N/m^3 (blue dots).

is doubled with respect to a single plate (see yellow lines on Figure 9). On the other hand, the analytical dispersion curves are obtained by minimizing the determinant of the system resulting from the boundary conditions in the perfect adhesion hypothesis (red full lines on Figure 2). The three-layer modes are labeled SH_0, SH_1, SH_2... according to ascending cut-off frequencies. There is a very good agreement between the two solving methods. One can consider that the model with a stiffness value of 10^{16} N/m^3 corresponds to a perfect adhesion. New sets of dispersion curves can be obtained, depending on the values of the stiffness. In Figure 3 are reported the dispersion curves for R_T equal to 10^{14}, 10^{15} and 10^{16} N/m^3. In the studied frequency bandwidth, the case of $R_T = 1015$ N/m^3 still describes a perfect bonding because the dispersion curves are superimposed on those for $R_T = 10^{16}$ N/m^3. There are

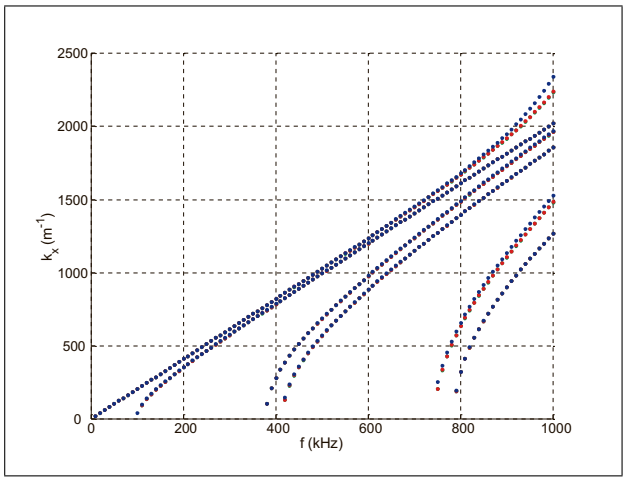


Figure 3. (Colour online) Numerical dispersion curves (Jones model) for $R_T = 10^{14}\,\mathrm{N/m^3}$ (blue dots), for $R_T = 10^{15}\,\mathrm{N/m^3}$ (red dots) and for $R_T = 10^{16}\,\mathrm{N/m^3}$ (green dots).

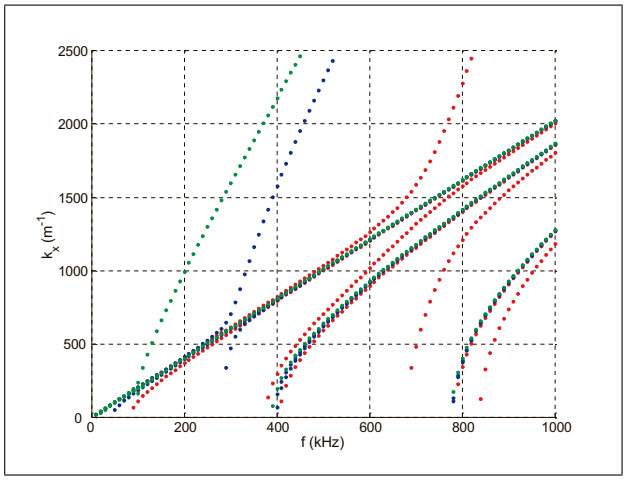


Figure 4. (Colour online) Numerical dispersion curves (Jones model) for $R_T = 10^{11}\,\mathrm{N/m^3}$ (green dots), for $R_T = 10^{12}\,\mathrm{N/m^3}$ (blue dots) and for $R_T = 10^{13}\,\mathrm{N/m^3}$ (red dots).

some slight differences between the dispersion curves for $R_T = 10^{14}\,\mathrm{N/m^3}$ and $R_T = 10^{16}\,\mathrm{N/m^3}$. So the case of RT=1014 $\mathrm{N/m^3}$ describes a slightly degraded bonding. On the other hand, a total delamination corresponds to values of R_T less than or equal to $10^{11}\,\mathrm{N/m^3}$ insofar as the dispersion curves obtained with these values are identical to those obtained in the case of a single aluminum plate with thickness $h = 4\,\mathrm{mm}$ (see red dots and yellow lines on Figure 9). In Figure 4 are reported the dispersion curves for R_T equal to 10^{11}, 10^{12} and $10^{13}\,\mathrm{N/m^3}$. In the studied frequency bandwidth, there are some slight differences between the dispersion curves for $R_T = 10^{11}\,\mathrm{N/m^3}$ (total delamination) and $R_T = 10^{12}\,\mathrm{N/m^3}$. So the case of $R_T = 10^{12}\,\mathrm{N/m^3}$ describes a slightly bonding. The aim is to compare these dispersion curves to the experimental ones, and to associate a stiffness value to each sample.

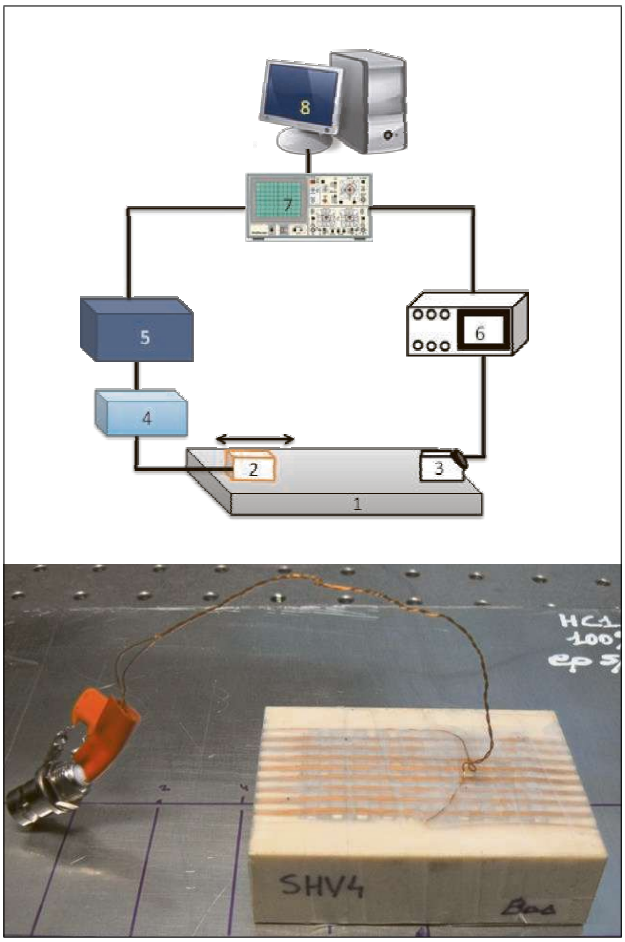


Figure 5. a. (Colour online) Experimental device: (1) Three-layer structure, (2) EMAT emitter transducer, (3) Piezocomposite receiver transducer on a plexiglas wedge, (4) Preamplifier, (5) Function generator, (6) Amplifier, (7) Oscilloscope, (8) Computer. b. (Colour online) EMAT transducer.

4. Experimental results and discussion

The experimental set-up is shown in Figure 5a. The emitter is an ElectroMagnetic Acoustic Transducer (EMAT - Figure 5b) manufactured in the laboratory. The magnetic elements periodicity is 8 mm corresponding to the wavenumber of the modes to be generated: $k_x = 785/\mathrm{m}$. Around this value of k_x, the SH_0 and SH_1 modes are too close to be experimentally distinguished, there are two other mode pairs (SH_2-SH_3 and SH_4-SH_5). Here, we focus on the SH_2-SH_3 mode pair. It is placed at 1 mm from the surface of the material (2 on Figure 5a) for a better power transmission. The receiver is a Valpey Fisher shear wave transducer of 500 kHz central frequency, placed on a Plexiglas wedge of 16° angle (3 on Figure 5a). The experiment is carried out with a quasi-harmonic excitation signal of ten cycles with a central frequency of $f = 560\,\mathrm{kHz}$ and 200 mV amplitude, delivered by an Agilent arbitrary waveform generator (5 on Figure 5a). It is 50 dB power-amplified (4 on Figure 5a), to optimize the EMAT response. The targeted modes to be generated are SH2 ($k = 785/\mathrm{m}$, $f = 530\,\mathrm{kHz}$), and SH_3 ($k = 785/\mathrm{m}$,

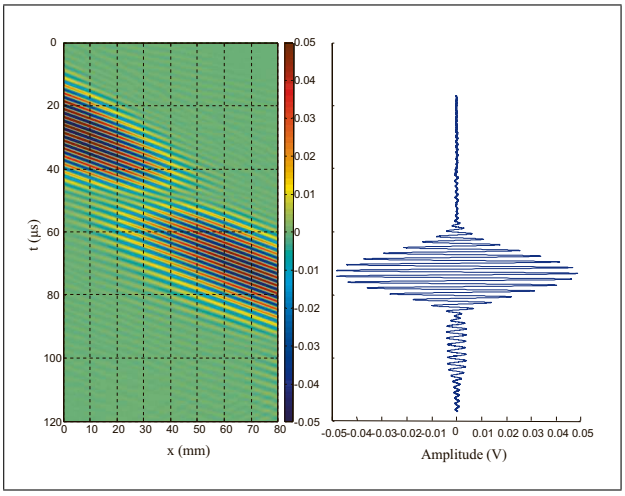


Figure 6. (Colour online) Left: time-space representation for the sample A100 (experimental result). The colour amplitude is in arbitrary unit. Right: an example of a temporal signal taken at the last position ($x = 80$ mm).

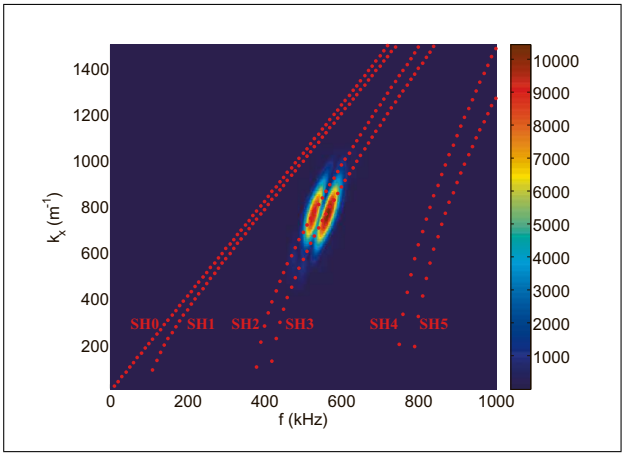


Figure 7. (Colour online) Wavenumber-frequency representation of the experimental signal for the sample A100 (experimental result). The colour amplitude is in arbitrary unit. Numerical dispersion curves (Jones model) for $R_T = 10^{16}$ N/m^3 (red dots).

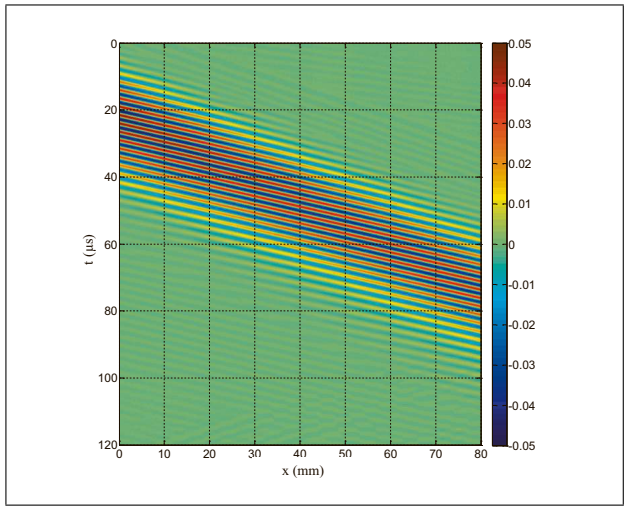


Figure 8. (Colour online) Time-space representation of the signal for the sample A70G30 (experimental result). The colour amplitude is in arbitrary unit.

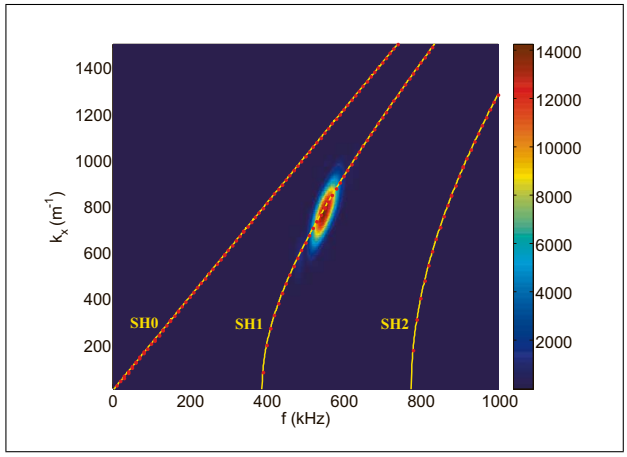


Figure 9. (Colour online) Wavenumber-frequency representation for the sample A70G30 (experimental result). The colour amplitude is in arbitrary unit. Red dots: numerical dispersion curves (Jones model) for $R_T = 10^{11}$ N/m^3 (red dots). Yellow lines: theoretical dispersion curves for one aluminium plate of 4 mm thick.

$f = 570$ kHz). The emitter is translated in the propagation direction, by steps of 0.1 mm, over 80 mm distance. For each position, the signal acquisition is done over 200 microseconds duration, corresponding to 20000 time samples. The size of the time-position matrix is thus 20000 rows and 800 columns. Figure 6 is a time-position representation of the experimental data collected for the A100 sample. It shows the propagation of two packs that correspond to two waves interfering during their propagation, as indicated by the vanishing zone in the middle of the representation. A double space-time FFT is performed for identification and comparison with the numerical dispersion curves. The temporal FFT is performed on 65536 points and the spatial FFT is performed on 16384 points. The aim is to respect the Nyquist-Shannon sampling theorem, which is largely the case here. We use the zero-padding technique to improve the localization of the maxima of the spectrum. In our case, the numbers of points allow to obtained a resolution of $\Delta f = 305$ Hz and $\Delta k = 7.7$/m, largely sufficient to determine with a good accuracy the frequency and the wavenumber that are of the order of 500–600 kHz and of 700–900/m respectively. Please note that the calculation of the 2D FFT with these numbers of points last less than one minute with a standard computer (processor Intel I5, 16 Go RAM). The result is presented on Figure 7. The numerical dispersion curves with a stiffness of $R_T = 11^{16}$ N/m^3 are superimposed in red. One can clearly identify the simultaneous propagation of the targeted SH_2 and SH_3 modes. Their simultaneous detection is allowed by the angular aperture of the receiver. A similar result is obtained for the A90G10, but not shown here for concision. The time-position representation for the A70G30 sample is given on Figure 8, and shows the propagation of a single mode, which is confirmed by the

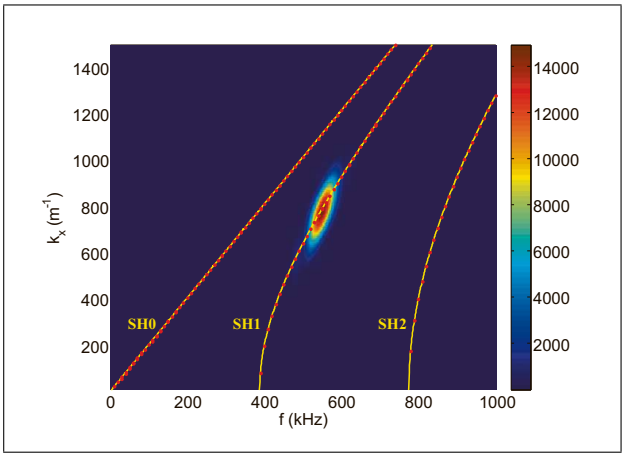


Figure 10. (Colour online) Wavenumber-frequency representation for the sample A50G50 (experimental result). The colour amplitude is in arbitrary unit. Red dots: numerical dispersion curves (Jones model) for $R_T = 10^{11}\,\mathrm{N/m^3}$ (red dots). Yellow lines: theoretical dispersion curves for one aluminium plate of 4 mm thick.

double FFT represented on Figure 9. The numerical dispersion curves with the parameters of the A70G30 sample and a stiffness of $R_T = 10^{11}\,\mathrm{N/m^3}$ are superimposed in red. A similar result is obtained for the A50G50 sample as shown on Figure 10. By increasing the grease ratio in the mixture, only one mode is found to propagate because the increasing ratio of grease in the glue introduces a total delamination, decoupling the two substrates. To verify this point, the theoretical dispersion curves of a single aluminium layer of 4 mm thick are plotted in yellow. There is a very good superimposition of the SH1 mode of a single layer and the experimental signal. One can conclude that there is a total delamination when the grease ratio is bigger than 30%.

5. Conclusions

The propagation of SH modes in a three-layer structure (metal-adhesive-metal) in which the adhesive is mixed with grease at different volume percentages, degrading progressively the adhesive quality and the coupling between the substrates, is studied. The dispersion curves for the SH modes in the different structures are first determined using the SAFE method. Experiments are finally carried out, using a set-up which allows measuring the surface displacement parallel to the surfaces of the plate. Analysis of the frequency-wavenumber representations of the experimental signals leads to the determination of different adhesion levels. In this work the close proximity of dispersion curves of a symmetric three-layer structure in perfect contact, was used as bonding quality indicator. The simultaneous propagation of two close modes is shown to provide rapid information on the bonding quality and then on the integrity of the whole three-layer structure. The propagation of only one mode in the same frequency-wavenumber range could indicate a weak bond or even a total delamination in the structure.

References

[1] L. Da Silva, A. Ochsner, R. Adams: Handbook of adhesion technology I, II. Springer, Berlin, 2011.

[2] B. A. Auld: Acoustic fields and waves in solids I. J. Wiley & Sons, New York, 1973.

[3] L. M. Brekhovskikh, O. A. Godin: Acoustics of layered media I. Springer, Berlin, 1990.

[4] J. D. Cheeke: Fundamentals and applications of ultrasonic waves. CRC Press LLC, 2002.

[5] C. C. H. Guyott, P. Cawley: The ultrasonic vibration characteristics of adhesive joints. J Acoust Soc Am **83** (1988) 632–640.

[6] P. B. Nagy, L. Adler: Non-destructive evaluation of adhesive joints by guided waves. J Appl Phys **66** (1989) 4658–4663.

[7] C. H. Yew, X. Weng: Using ultrasonic sh waves to estimate the quality of adhesive bonds in plate structures. J Acoust Soc Am **77** (1985) 1813–1823.

[8] B. Le Crom, M. Castaings: Shear horizontal guided wave modes to infer the shear stiffness. J Acoust Soc Am **127** (2010) 2220–2230.

[9] R. Adams, B. Drinkwater: Nondestructive testing of adhesively-bonded joints. NDT&E Int **30** (1997) 93–98.

[10] M. Lowe, P. Cawley: The applicability of plate wave techniques for the inspection of adhesive and diffusion bonded joints. J Nondestr Eval **13** (1994) 185–200.

[11] T. Kundu, K. Maslov: Material interface inspection by lamb waves. Int J Sol Struct **34** (1997) 3885–3901.

[12] F. Coulouvrat, M. Rousseau, O. Lenoir, J. L. Izbicki: Lamb-type waves in a symmetric solid-fluid-solid trilayer. Acta Acust united Ac **84** (1998) 12–20.

[13] K. Heller, L. J. Jacobs, J. Qu: Characterization of adhesive bond properties using Lamb waves. NDT&E Int **33** (2000) 555–563.

[14] S. Barros, A. Gama, M. Rousseau, B. Collet: Characterization of bonded plates with Lamb and SH waves using a quasi-static approximation. Latin Am J Sol Struct **1** (2004) 379–399.

[15] C. Brotherhood, B. Drinkwater, S. Dixon: The detectability of kissing bonds in adhesive joints using ultrasonic techniques. Ultrasonics **41** (2003) 521–529.

[16] F. Lanza di Scalea, P. Rizzo: Propagation of ultrasonic guided waves in lap-shear adhesive joints: Case of incident A0 Lamb wave. J Acoust Soc Am **115** (2004) 146–157.

[17] J. Allin, P. Cawley, M. Lowe: Adhesive disbond detection of automotive components using first mode ultrasonic resonance. NDT&E Int **36** (2003) 503–514.

[18] J. P. Jones, J. S. Whittier: Waves at a flexibly bonded interface. J Appl Mech **34** (1967) 905–909.

[19] S. I. Rokhlin, Y. J. Wang: Analysis of boundary conditions for elastic waves interaction with an interface between two solids. J Acoust Soc Am **89** (1991) 503–515.

[20] V. Vlasie, S. de Barros, M. Rousseau, L. Champaney: Ultrasonic rheological model of cohesive and adhesive zones in aluminum joints: Validation by mechanical tests. Arch Appl Mech **75** (2006) 220–234.

[21] M. Koshiba, K. Hasegawa, M. Suzuki: Finite-element solution of horizontally polarized shear wave scattering in an elastic plate. IEEE T Ultrasons Ferr Freq Cont **34** (1987) 461–466.

[22] B. Hosten, M. Castaings: Finite elements methods for modeling the guided waves. J Acoust Soc Am **117** (2005) 1108–1113.

[23] A. Marzani, E. Viola, I. Bartoli, F. L. D. Scaela, P. Rizzo: A semi-analytical finite element formulation for modeling stress wave propagation in axisymmetric damped waveguides. J Sound Vib **318** (2008) 488–505.

[24] Z. A. B. Ahmad, U. Gabbert: Simulation of Lamb wave reflections at plate edges using the semi-analytical finite element method. Ultrasonics **52** (2012) 815–820.

[25] N. Ismaili, D. Chenouni, Z. Lakhliai, M. El-Kettani, B. Morvan, J. L. Izbicki: Determination of epoxy film parameters in a three-layer metal/adhesive/metal structure. IEEE Trans Ultrason Ferroelectr Freq Control **56** (2009) 1955–1959.

[26] M. V. Predoi, M. Ech-Cherif El-Kettani, D. Leduc, P. Pareige, K. Coné: Use of shear horizontal waves to distinguish adhesive thickness variation from reduction in bonding strength. J Acoust Soc Am **138** (2015) 1206–1213.

[27] S. Dixon, E. C. Palmer, S. Palmer: A laser-EMAT system for ultrasonic weld inspection. Ultrasonics **37** (1999) 273–281.

[28] J. Brenstein, J. Spicer: Hybrid laser/broadband EMAT ultrasonic system for characterization cracks in metals. J Acoust Soc Am **111** (2002) 1685–1691.

[29] P. Jiang, R. E. Apfel, E. C. Everbach: Mixture laws for ultrasonic tissue characterization. J Acoust Soc Am **87** (1990) 115.

[30] J. Ding, B. Wu, C. He: Reflection and transmission coefficients of the SH0 mode in the adhesive structures with imperfect interface. Ultrasonics **70** (2016) 248–257.

[31] M. Ech-Cherif El-Kettani, D. Leduc, C. Potel, M. Bruneau, L. Foze, M. V. Predoi: Effects of the interface roughness in metal-adhesive-metal structure on the propagation of shear horizontal waves. J Acoust Soc Am **141** (2017) 4591–4599.

[32] C. Gauthier, M. Ech-Cherif El-Kettani, J. Galy, M. V. Predoi, D. Leduc, J.-L. Izbicki: Lamb waves characterization of adhesion levels in aluminum/epoxy bi-layers with different cohesive and adhesive properties. Int. J. Adhesion Adhesives **74** (2017) 15–20.

[33] COMSOL Multiphysics: User manual. https://www.comsol.com/. Last visited 08.2017.

[34] V. Vlasie, M. Rousseau: Acoustical validation of the rheological models for a structural bond. Wave motion **37** (2003) 333–349.